

# A Single Motor Driving and Steering Mechanism for a Transformable Bicycle

Kazuki Sekine<sup>a</sup> and Ikuo Mizuuchi<sup>b</sup>

Tokyo University of Agriculture and Technology, 2-24-16 Naka-cho, Koganei-shi, Tokyo 184-8588, Japan

**Keywords:** Single Motor, Driving and Steering Mechanism, Self-driving Bicycle, Transforming Mechanism.

**Abstract:** This research aims to propose a bicycle capable of transforming into a stable form suitable for autonomous driving, and achieving both driving and steering with a single motor, using differential drive method. A novel mechanism of one-motor differential drive using bevel gears and one-way clutches was devised. Then, a prototype without transforming mechanism was fabricated. An experiment was conducted to demonstrate that differential drive with a single motor is possible. In the experiment, the prototype was capable of running in straight lines and curves with small meandering. Next, to formulate the deceleration of the non-drive side wheel in the proposed drive mechanism, another series of experiments was conducted. The equation for the change in wheel rotating speed derived from the results enables accurate estimation of the future position of the prototype, allowing it to run autonomously in further research.

## 1 INTRODUCTION

This research aims to transform a bicycle into a stable form suitable for autonomous driving and to combine driving and steering with a single motor.

Shared-cycle services are convenient because bicycles can be easily rented, but they require the bicycles to be returned after use. However, the collection of abandoned bicycles and the redistribution and rearrangement of excess bicycles at specific return ports are performed by trucks and other human operators, which reduces the profitability of the shared-cycle business. Therefore, we consider installing an autonomous driving function in bicycles to automatically return and relocate bicycles.

In existing research examples of autonomous bicycles, such as Yeh et al. (Ting-Jen Yeh and Tseng., 2019), two or more motors are used for driving and steering, which makes the mechanism complex and causes many failure factors. This makes them unsuitable for use as shared bicycles, which are used in large numbers and for long periods. In addition, autonomous driving in the form of a bicycle requires some kind of stabilizing mechanisms such as gyroscopic mechanism or large landing gears. Even with those mechanism, there is always a risk of falling. Also, those mechanisms only make the bicycle heavier and become an obstacle when it is pedaled by a hu-

man. So, transforming the bicycle into a stable form and drive autonomously with a single motor is an effective way. Nalao et al. (Sánchez et al., 2020) developed an autonomous bicycle with two rear wheels with variable tread. When the bicycle is driven by human power, the rear wheels are attached to enable the bicycle to tilt and turn. When it drives autonomously, the tread is widened to stabilize. However, the variable tread mechanism requires multiple actuators and complex mechanisms to deploy, making it impractical.

Robots driven and steered by a single motor already exist. Ito et al. (Ito et al., 2019) developed a single motor robot with passive wheels and propelled by yaw moment generated by rotating weights. However, passive wheels limit the ability of robots such as overcoming steps. So, application to a bicycle is difficult. Peidr o et al. (Peidr o et al., 2019) developed a robot with two magnetic or pneumatic adhesion pads at the bottom of each of the two ends. It can pivot about different axes by alternately releasing or attaching these pads to the floor. However, magnetic adhesion is possible only on a ferromagnetic medium, and pneumatic adhesion needs a vacuum pump, which requires additional energy. Ribas et al. (Ribas et al., 2007) developed a three-wheeled robot that only front wheel is connected to motor. The front wheel is passively steered by the direction of its rotation. However, the front wheel always faces almost sideways to the body, which interferes with the straight-line motion of the robot. Toyozumi et al. (Toyoizumi et al.,

<sup>a</sup>  <https://orcid.org/0000-0003-3727-8690>

<sup>b</sup>  <https://orcid.org/0000-0003-4657-2613>

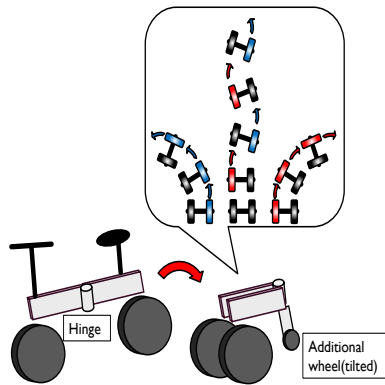


Figure 1: Conceptual diagram.

2010) developed a spherical robot that can generate both translational and rotational motion with one motor. However, the spherical shape is unstable and easily changes its posture when external force is applied, making it impossible to climb a slope. Zarrouk et al. (Zarrouk and Fearing, 2015) developed a hexapod robot driven and steered by a single motor. The robot has two active legs and four passive legs. Cheng et al. (Cheng et al., 2010) developed a single-motored soft crawling robot using thermorheological (TR) fluids for modulating the stiffness of its body locally to change the bending position and direction of it. However, additional energy is required to heat the fluid, and the use of tendons for drive makes it difficult to apply this mechanism to a wheeled robot. Dharmawan et al. (Dharmawan et al., 2017) developed a four-legged robot driven by a single piezoelectric unimorph actuator and capable of moving forward and turning left or right. However, the driving principle assumes a legged robot and is difficult to apply to a wheeled robot. Also, piezoelectric actuators can only produce very small displacements and require high voltage, so it can be dangerous.

In this study, we consider using the mechanism of a folding bicycle to transform the bicycle into a stable form suitable for autonomous driving, and to combine driving and steering with a single motor.

## 2 REALIZATION METHOD

A conceptual diagram of this study is shown in Figure 1. The following conditions are necessary to achieve the goals of this study.

- Develop a drive mechanism achieving both driving and steering by a single motor.
- Apply the drive mechanism to a bicycle.

### 2.1 The Driving and Steering Mechanism by a Single Motor

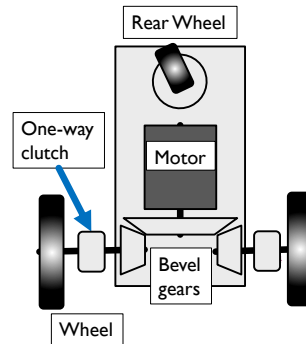


Figure 2: The proposed drive mechanism.

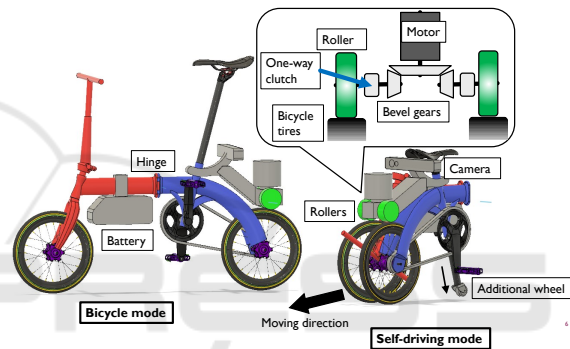


Figure 3: The 3D modeled transformable bicycle.

In this research, we chose the differential drive (Dudek and Jenkin, 2010) as a driving method, which is commonly used as a drive method for two-wheeled robots. This method uses the difference in rotational speeds of the left and right wheels to drive and steer the robot at the same time. In the conventional differential drive, each of the left and right wheels has a motor. In this research, a new mechanism was developed to realize differential drive with a single motor. The proposed drive mechanism is shown in Figure 2. In this mechanism, the motor torque is distributed to the independent left and right drive shafts through bevel gears. As a result, the left and right drive shafts rotate in opposite directions. Wheels are then attached to the left and right drive shafts via one-way clutches. The one-way clutch is a mechanism that transmits torque in only one direction of rotation. So, for each direction of rotation of the motor, only one of the left and right wheels rotates in the forward direction. Therefore, by rotating the motor to forward and reverse directions in turn, differential drive is possible with the limitation that the left and right wheels cannot be driven simultaneously.

## 2.2 Application of the Drive Mechanism to a Bicycle

For the application of the drive mechanism to a bicycle, a folding bicycle that can be folded from the center of its frame was chosen. Figure 3 shows the 3D modeled transformable bicycle. When folded, the front and rear wheels of the bicycle face each other on the right and left sides, so that the robot can easily stand on its own by adding an wheel to the tail section. The tread, which is an important factor for the stability of a two-wheeled robot, can be easily adjusted by changing the opening of the hinge used in the folding process. When the bicycle is pedaled by a human, the motor drives the rear wheel via a roller. when the bicycle is folded, the front wheel also contacts the other roller, and both wheels are driven with the differential drive method. The bicycle drives autonomously using on-board cameras to recognize their surroundings.

## 3 MODELING OF DYNAMICS AND KINEMATICS OF ROBOT

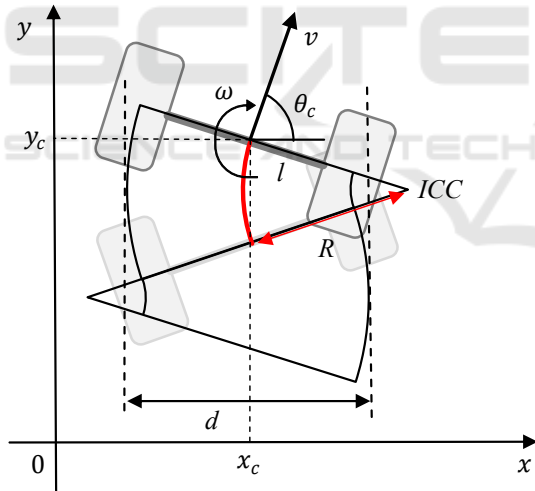


Figure 4: The kinematics of two-wheeled robot.

### 3.1 Modeling of Kinematics

The kinematics of the robot is modeled by considering the self-localization using inverse kinematics calculations based on the wheel rotation speeds. First, consider modeling the dynamics of the robot moving on a  $xy$ -plane as shown in Figure 4. Let  $\mathbf{q} = [x_c \ y_c \ \theta_c]^T$  be a vector consisting of the absolute positions  $x_c, y_c$  of the robot and the declination  $\theta_c$  from the  $x$ -axis. Given the nonholonomic constraint that

the wheels do not slip or skid, the constraints are imposed by the following equation.

$$\dot{x}_c \sin \theta_c - \dot{y}_c \cos \theta_c = 0 \quad (1)$$

Let  $v$  be the translation velocity of the robot and  $\omega$  be the rotation velocity,  $\dot{\mathbf{q}}$  is given by the following equation.

$$\dot{\mathbf{q}} = \begin{bmatrix} \cos \theta_c & 0 \\ \sin \theta_c & 0 \\ 0 & 1 \end{bmatrix} \begin{bmatrix} v \\ \omega \end{bmatrix} \quad (2)$$

In the previous equation, the vector  $[v \ \omega]^T$  is given by :

$$\begin{bmatrix} v \\ \omega \end{bmatrix} = \frac{r}{2} \begin{bmatrix} 1 & 1 \\ \frac{2}{l} & -\frac{2}{l} \end{bmatrix} \begin{bmatrix} \dot{\theta}_l \\ \dot{\theta}_r \end{bmatrix} \quad (3)$$

where  $r$  is the wheel radius,  $l$  is the tread, and  $\dot{\theta}_l$  and  $\dot{\theta}_r$  are the angular velocities of the left and right wheels, respectively. From Equation (2), (3), the following equation is derived.

$$\dot{\mathbf{q}} = \frac{r}{2} \begin{bmatrix} \cos \theta_c & \cos \theta_c \\ \sin \theta_c & \sin \theta_c \\ \frac{2}{l} & \frac{2}{l} \end{bmatrix} \begin{bmatrix} \dot{\theta}_l \\ \dot{\theta}_r \end{bmatrix} \quad (4)$$

Therefore, the state of the vehicle body  $\mathbf{q}(t)$  at a certain time  $t$  is given by the following equation.

$$x_c(t) = \frac{r}{2} \int_t^0 (\dot{\theta}_l + \dot{\theta}_r) \cos \theta_c(t) dt \quad (5)$$

$$y_c(t) = \frac{r}{2} \int_t^0 (\dot{\theta}_l + \dot{\theta}_r) \sin \theta_c(t) dt \quad (6)$$

$$\theta_c(t) = \frac{r}{l} \int_t^0 (\dot{\theta}_l - \dot{\theta}_r) dt \quad (7)$$

During driving, the robot travels in a curve centered at the Instantaneous Center of Curvature (ICC) due to the difference in rotational speeds of the left and right wheels, as shown in Figure 4. In this case, the radius  $R$  of the arc is given by the following equation.

$$R = \frac{l(\dot{\theta}_l + \dot{\theta}_r)}{2(\dot{\theta}_l - \dot{\theta}_r)} \quad (8)$$

When a robot drive using differential drive by single motor, the robot always meandering because it has a constraint that the both wheels cannot be driven at the same time. This meandering shortens the distance the robot can reach. Therefore, in single-motor differential drive, it is important to minimize it. In modeling meandering, I defined the meandering rate  $D = \frac{d-l}{l}$ .  $D = 0$  when the robot is driving straight. Here,  $d$  is defined as follows.

$$d = \frac{l}{\theta_l - \theta_r} \left( 2\theta_l - (\theta_l + \theta_r) \cos \frac{r(\theta_l - \theta_r)}{2l} \right) \quad (9)$$

### 3.2 Modeling of Dynamics

In the proposed driving mechanism, the left and right wheels are driven alternately, so the wheel on the non-driven side continues to rotate due to inertia and gradually decelerates due to the resistance torque received from the ground and the drive system. Therefore, accurate estimation of  $q$  at a given time requires modeling of the wheel motion. If the rotation angle of the wheel is  $\theta$ , the equation of wheel motion is given by the following equation.

$$I\ddot{\theta} = \tau - \tau_v(\dot{\theta}) - \tau_f \quad (10)$$

$$\tau_v(\dot{\theta}) = c_v\dot{\theta} \quad (11)$$

where  $I$  is the moment of inertia including that of the robot body,  $\tau$  is the drive torque of the wheel by the motor,  $\tau_v(\dot{\theta})$  is the viscous torque, and  $c_v$  is the viscous coefficient.  $\tau_f$  is the friction torque. From these equations, the wheel rotation angle  $\theta$  is expressed by the following equation:

$$\theta(t) = A \exp\left(-\frac{c_v}{I}t\right) - \frac{\tau_f}{c_v}t + B \quad (12)$$

where  $A, B$  are integral constants. If the initial angle and angular velocity of the wheel at  $t = 0$  are  $\theta_0, \dot{\theta}_0$ , Equation (12) is expressed as follows.

$$\theta(t) = K \exp\left(-\frac{c_v}{I}t\right) - \frac{\tau_f}{c_v}t + \theta_0 - K \quad (13)$$

$$K = -I(c_v\dot{\theta}_0 + \tau_f)$$

To accurately predict the robot's future position, each coefficient in Equation (13) must be estimated by experiment.

## 4 DEVELOPMENT OF A ROBOT FOR DEMONSTRATION OF DRIVING METHOD

To demonstrate the proposed drive system, a robot without a folding mechanism was fabricated. Figure 5 shows the structure of the 3D modeled robot and the developed robot is shown in Figure 6. The robot is equipped with one Futaba RS406CB serial servo module. The maximum torque  $\tau_{max}$  is 28.0 kg·cm. The motor is connected to left and right drive shafts via bevel gears with a gear ratio of 2:1, as shown in Figure 7. Therefore, the rotation angles of the wheels are twice the motor rotation angle. The robot has two 70 mm radius wheels. The power source is an 11.1V 2100mAh Li-Po battery. The servo module is connected to an onboard Raspberry Pi 3 Model B controller via an RSC-U485 USB-RS485 converter.

The robot autonomously drives after receiving commands from an external PC connected to Raspberry Pi using Wi-Fi. The wheels are 3D printed using Tough PLA filament and attached to the drive shafts via Tsubaki BB15-2K-K cam clutches, as shown in Figure wheel. The friction torque of the cam clutch is 0.010 Nm. The tires are 3D printed using Formlabs Elastic 50A Resin. Two Copal RE12D300 Rotary encoders are attached to the left and right wheels via 15mm radius rollers. Rubber bands are used to press the rollers against the wheels to keep them from slipping, as shown in Figure 9. The output signal of each rotary encoder is counted by the MIKROE-1917 encoder count board and sent to the Raspberry Pi via SPI communication. Inverse kinematics calculations are performed to estimate the  $q$  of the robot at a given time based on the angle time series obtained from the encoders.

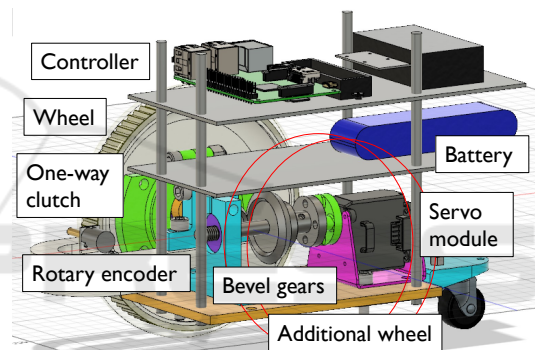


Figure 5: The structure of the 3D modeled robot.

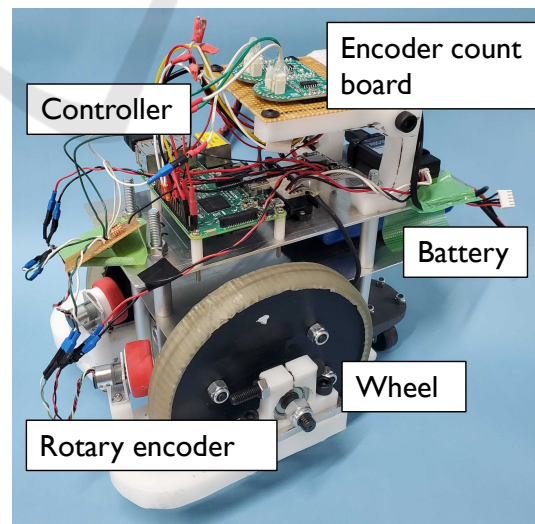


Figure 6: The developed robot.

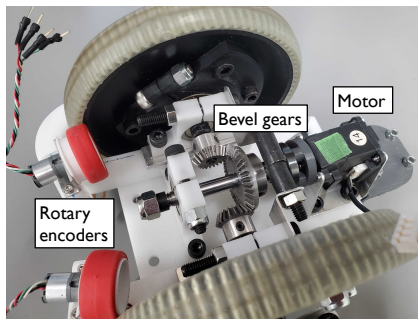


Figure 7: The drivetrain of the robot.

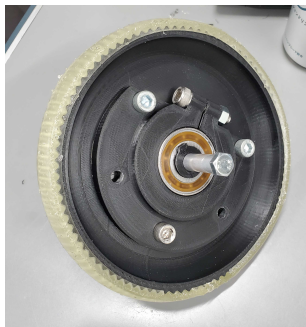


Figure 8: The wheel assembly.

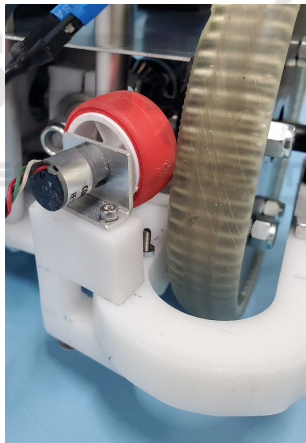


Figure 9: The rotary encoder attached to wheel via roller.

## 5 EXPERIMENTS

### 5.1 Demonstration Test of Differential Drive with a Single Motor

A driving test was conducted to demonstrate the possibility of driving with differential drive, as shown in Figure 10. First, the servo module is set to command mode. In this mode, the target angle and rotating time can be set using program commands. Then, running the motor with the target rotation angle and measur-

ing the wheel rotation angle at 10 ms intervals using rotary encoders.

In this experiment, the robot did the three types of movements shown below.

- Straight ahead
- Left curve
- Right curve

In the straight movement, the motor alternated between 20 deg CW and 20 deg CCW rotation at 1 s intervals. In the left curve movement, the motor alternated between 20 deg CW and  $k \cdot 20$  deg CCW rotation 15 times at 1 s intervals.  $k$  is a coefficient less than 1, in this case  $k = 0.5$ . This means that the left wheel has less rotation angle than the right wheel. In the right curve movement, the motor alternated between  $k \cdot 20$  deg CW and 20 deg CCW rotation 15 times at 1 s intervals. This means that the right wheel has less rotation angle than the left wheel. Combining these movements, the robot was made to run in the following order: straight ahead, two curves (left, right), then straight ahead. The experiment was filmed by a camera fixed near the ceiling. Then, an open-source motion analysis software Kinovea was used to extract the actual trajectory of the robot from the recorded video and draw it as a line. The trajectory is compared with the trajectory calculated from the rotation angle measured by rotary encoders. The actual trajectory is shown in Figure 11 and the calculated trajectory is shown in Figure 12. The calculated trajectory matched well with the actual trajectory, but a difference in orientation occurred in the middle of the right curve. This may be caused by the accumulated errors in the estimated orientation of the robot, due to the wheels slipping against the floor. The reducing of the accumulated errors is needed for better self-localization.

From this experiment, the proposed drive system was verified by the fact that the machine was able to move forward while meandering and make left and right curves.

### 5.2 Estimation of the Drag Coefficients of the Robot

In the experiment in Subsection 5.1, the target time series of the motor rotation angle  $\theta_m$  was decided without considering the robot to reach a specific target position. To reach a target point, path planning is needed. For accurate path planning, the estimation of each drag coefficient  $c_v, \tau_f$  in Equation (13) is needed.

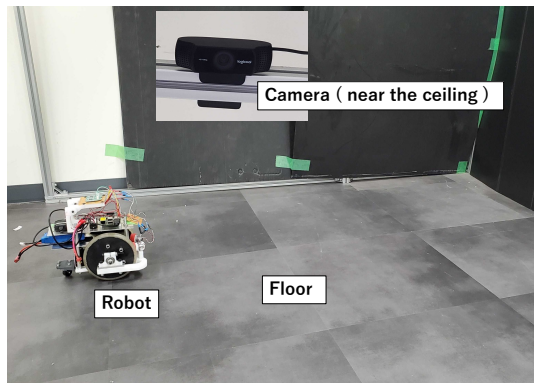


Figure 10: Driving test of the robot.

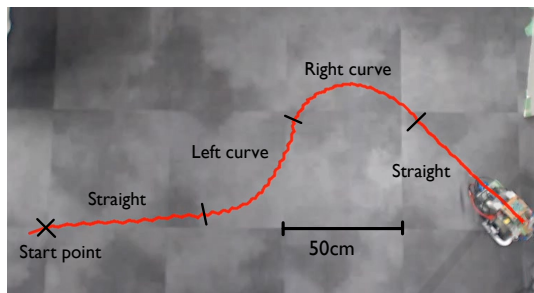


Figure 11: The actual trajectory of the robot.

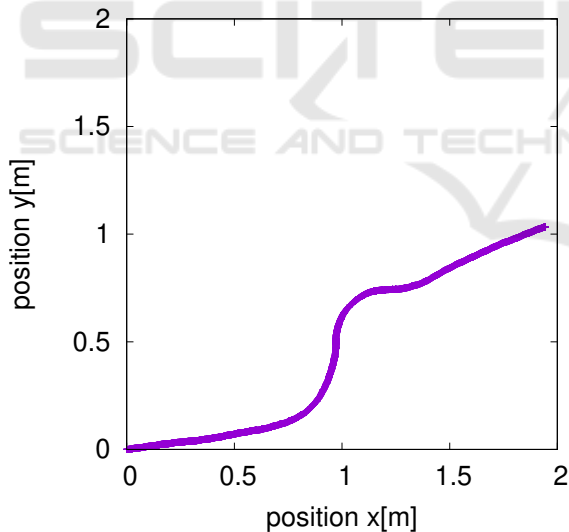


Figure 12: The calculated trajectory of the robot.

### 5.2.1 Estimation When Driving on Curves

An experiment was conducted to estimate each drag coefficient of the robot. First, the robot was put on a flat floor. Then, one of the wheels is accelerated by the motor from a standstill to 7 different initial rotating velocities by setting target angles for the motor in 10 deg increments from 10 deg to 70 deg. Then, the time variation of wheel rotation angle  $\theta$  and wheel

rotation velocity  $\dot{\theta}$  is recorded by the rotary encoder from the moment the motor drive torque  $\tau$  reaches 0 to the moment the wheel comes to a stop. The result of experiment is shown in Figure 13-16. The black lines in Figure 15,16 shows the exponential fitting of the 'target angle = 70 deg' datas, and the black lines in Figure 13,14 shows the exponential fitting of the 'target angle = 70 deg' datas.

From these data, the angles and angular velocities of the left and right wheels  $\theta_L, \theta_R, \dot{\theta}_L, \dot{\theta}_R$  can be approximated by the following equations.

$$\begin{aligned} \theta_L(t) &= -7 \times 10^3 \exp(-3 \times 10^{-3}t) - 20t + 7 \times 10^3 \\ \dot{\theta}_L(t) &= 20 \exp(-3 \times 10^{-3}t) - 20 \\ \theta_R(t) &= -9 \times 10^6 \exp(-5 \times 10^{-5}t) - 700t + 9 \times 10^6 \\ \dot{\theta}_R(t) &= 700 \exp(-7 \times 10^{-5}t) - 700 \end{aligned} \quad (14)$$

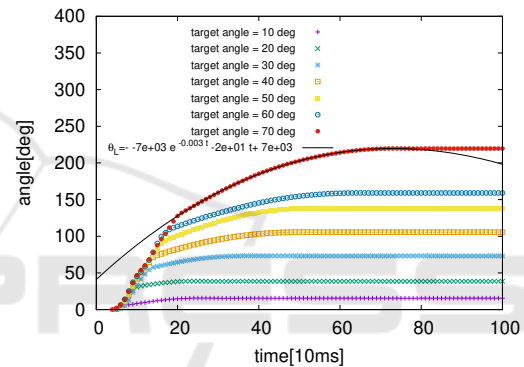


Figure 13: Time variation of angle of left wheel.

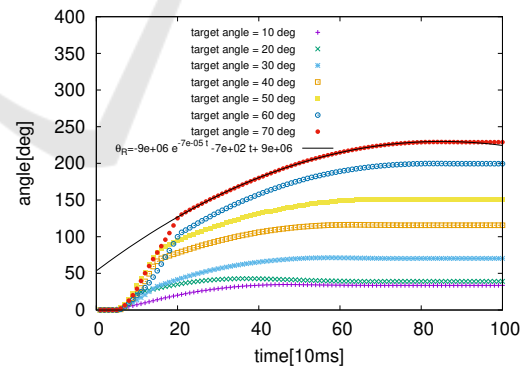


Figure 14: Time variation of angle of right wheel.

### 5.2.2 Estimation When Driving Straight

To see if there is a difference, an experiment was conducted in straight-line driving conditions to compare to the former experiment. A 25 deg slope was set on the floor, as shown in Figure 17. The robot was held by hand at a position on the slope, at a height of 10 cm from the ground. When the hand was released, the robot was accelerated by gravity down the slope

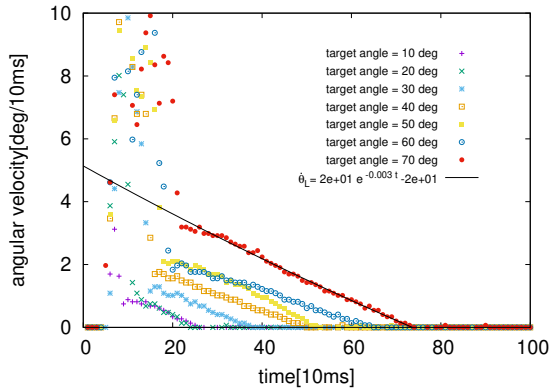


Figure 15: Time variation of angular velocity of left wheel.

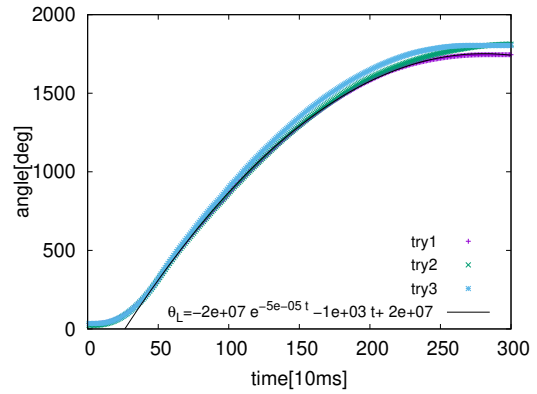


Figure 18: Time variation of angle of left wheel.

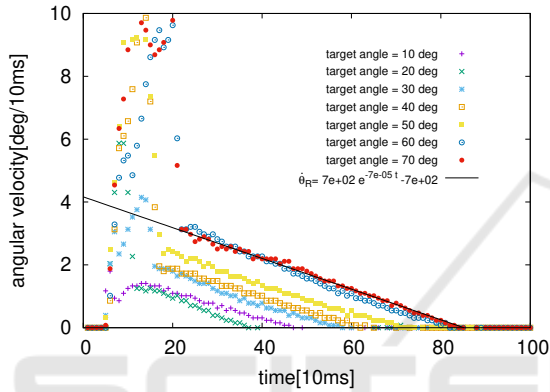


Figure 16: Time variation of angular velocity of right wheel.

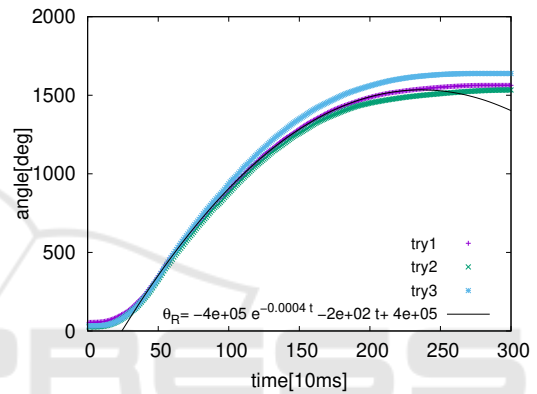


Figure 19: Time variation of angle of right wheel.

and traveled by inertia on the flat floor. The angle of rotation of the wheels was measured with rotary encoders until the robot came to a stop. The result of experiment is shown in Figure 18-21. The black lines in Figure 15,16 shows the exponential fitting of the 'try 1' data, and the black lines in Figure 13,14 shows the exponential fitting of the 'try 1' data. From these data,  $\theta$  and  $\dot{\theta}$  can be approximated by the following equations.

$$\begin{aligned} \theta_L(t) &= -2 \times 10^7 \exp(-5 \times 10^{-5} t) - 100t + 2 \times 10^7 \\ \dot{\theta}_L(t) &= 413 \exp(-1.4 \times 10^{-4} t) - 397 \\ \theta_R(t) &= -4 \times 10^5 \exp(-4 \times 10^{-4} t) - 200t + 4 \times 10^5 \\ \dot{\theta}_R(t) &= 59 \exp(-1.2 \times 10^{-3} t) - 43 \end{aligned} \quad (15)$$

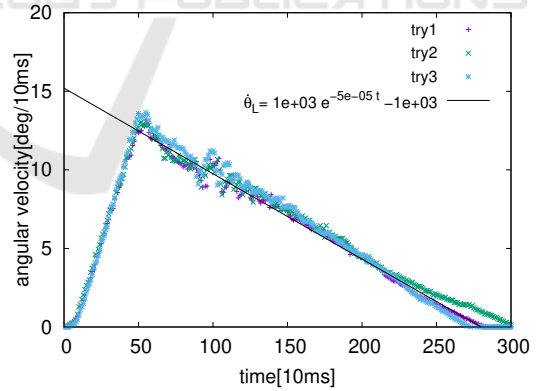


Figure 20: Time variation of angular velocity of left wheel.

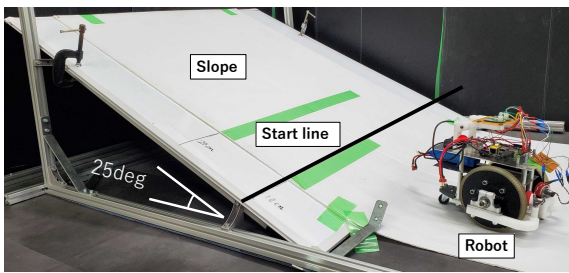


Figure 17: The slope used in the straight-line experiment.

### 5.2.3 Discussion

The results of these two experiments follow that the deceleration of wheel rotations is faster in curved driving conditions than in straight one. This may be caused by the fact that the rotation angle of the non-driven wheels were very small when traveling in curves, causing friction in the direction of yaw rotation of the robot.

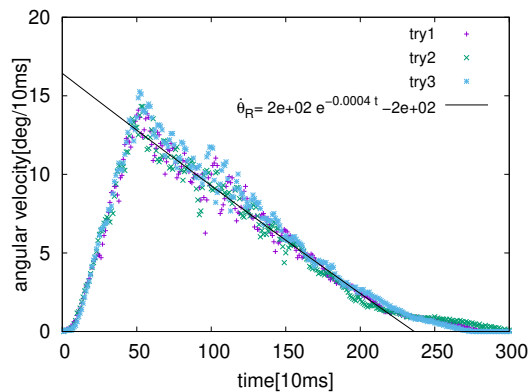


Figure 21: Time variation of angular velocity of right wheel.

## 6 CONCLUSIONS

In this study, we proposed a method to transform a bicycle into a stable form suitable for autonomous driving and achieve both drive and steer with a single motor. A prototype without a transforming mechanism was built and tested to demonstrate the proposed driving method and the driving trajectory estimation method. We are planning to construct an algorithm for reaching a goal position and to demonstrate the algorithm using the prototype. In addition, a regenerative mechanism to reduce energy loss due to acceleration and deceleration is planned to be installed in the prototype. Furthermore, we plan to fabricate a robot with a transforming mechanism using a folding bicycle and conduct driving tests in an environment that simulates an actual urban area.

## REFERENCES

- Cheng, N., Ishigami, G., Hawthorne, S., Chen, H., Hansen, M., Telleria, M., Playter, R., and Iagnemma, K. (2010). Design and analysis of a soft mobile robot composed of multiple thermally activated joints driven by a single actuator. In *2010 IEEE International Conference on Robotics and Automation*, pages 5207–5212.
- Dharmawan, A. G., Hariri, H. H., Foong, S., Soh, G. S., and Wood, K. L. (2017). Steerable miniature legged robot driven by a single piezoelectric bending unimorph actuator. In *2017 IEEE International Conference on Robotics and Automation (ICRA)*, pages 6008–6013.
- Dudek, G. and Jenkin, M. (2010). *Computational Principles of Mobile Robotics*. Cambridge University Press, USA, 2nd edition.
- Ito, S., Niwa, K., Sugiura, S., and Morita, R. (2019). An autonomous mobile robot with passive wheels propelled by a single motor. *Robotics and Autonomous Systems*, 122:103310.
- Peidró, A., Gallego, J., Payá, L., Marín, J. M., and Reinoso, Ó. (2019). Trajectory analysis for the masar: A new modular and single-actuator robot. *Robotics*, 8:78.
- Ribas, L., Mujal, J., Izquierdo, M., and Ramon, E. (2007). Motion control for a single-motor robot with an undulatory locomotion system. In *2007 Mediterranean Conference on Control and Automation*, pages 1–6.
- Sánchez, N. C., Pastor, L. A., and Larson, K. (2020). Autonomous bicycles: A new approach to bicycle-sharing systems. *2020 IEEE 23rd International Conference on Intelligent Transportation Systems (ITSC)*, pages 1–6.
- Ting-Jen Yeh, H.-T. L. and Tseng, P.-H. (2019). Balancing control of a self-driving bicycle. In *ICINCO*.
- Toyoizumi, T., Yonekura, S., Kamimura, A., Tadakuma, R., and Kawaguchi, Y. (2010). 1-dof spherical mobile robot that can generate two motions. In *2010 IEEE/RSJ International Conference on Intelligent Robots and Systems*, pages 2884–2889.
- Zarrouk, D. and Fearing, R. S. (2015). Controlled in-plane locomotion of a hexapod using a single actuator. *IEEE Transactions on Robotics*, 31(1):157–167.